Settling and rising dynamics of river litter

James Lofty[1*], Daniel Valero[2], Mário J. Franca[1]

[1]Institute for Water and Environment (IWU), Karlsruhe Institute of Technology (KIT), Karlsruhe, Germany

[2]Department of Civil and Environmental Engineering, Imperial College London, London, UK

*Corresponding author (james.lofty@kit.edu)

This is a non-peer reviewed preprint submitted to EarthArXiv

Manuscript submitted for publication in *Environmental Science & Technology*

Abstract

Global assessments of river litter transport, accumulation, and export to the oceans remain constrained because the particle-scale hydrodynamic variables governing litter movement are currently unknown. We resolve this by explaining the vertical dynamics of full-scale river litter in quiescent water through multi-camera, three-dimensional trajectory reconstructions of over a thousand litter items spanning 24 River-OSPAR categories, representing ~80% of observed riverine litter. Our results show that settling and rising velocities span three orders of magnitude (−82.1 to −0.29 cm s^{-1} and 0.90 to 143.3 cm s^{-1}, respectively), indicating large variability in transport among litter categories. Despite the wide variability of velocities, drag coefficients were relatively consistent, with a median value of 1.03 and interquartile range spanning 0.45 to 1.72. We identify four trajectory regimes – straight vertical, straight oblique, nonlinear vertical, and nonlinear oblique – establishing a regime map based on particle Reynolds number and litter anisotropy. We further propose a mechanistic explanation for the four regimes, arising from the coupled effects of wake dynamics and litter physical properties. These results provide the parameterisation required for predictive, physics-based models of river litter transport.

1 Introduction

Anthropogenic litter, particularly plastic pollution, poses significant consequences for biodiversity [1], water resources [2], flooding [3] and the economy [4]. Rivers function as both conveyors

and sinks for litter from land-based sources [5,6]. Effectively mitigating the problem requires a predictive understanding of where and when litter is mobilised, transported or accumulates. Resolving this relies on hydrodynamic models capable of simulating litter movement [7–9]. However, hydrodynamic models based on advection-diffusion equations are fundamentally limited by the lack of parameterisation of the particle-scale variables that govern litter transport and dispersion: settling and rising velocities, drag coefficients, transverse motions and trajectory dynamics. Without these key variables, litter transport predictions remain highly uncertain [10], limiting our ability to identify accumulation zones, quantify riverine plastic fluxes and design effective monitoring and mitigation strategies.

While the settling and rising dynamics are well understood for spheres [11–13], cylinders [14] disks [15,16], and plates [17,18], and extensive datasets exist for the vertical velocities of microplastics (plastics < 5 mm in size) [19–22], they remain largely unquantified for highly heterogeneous objects such as riverine litter. The few existing litter experiments typically rely on idealised geometries and limited sample sizes [23–25], which do not represent the extreme geometric diversity of real riverine litter [26] and are insufficient to explain the inherent variability of litter transport [7]. Anisotropic particles exhibit diverse behaviours in quiescent waters [27], including significant lateral drifting motion and oscillatory or chaotic trajectories. These complex motions enhance dispersion [28], causing variability in transport predictions that cannot be explained by a single vertical velocity [7,29]. For canonical objects, distinct trajectory regimes have been systematically mapped, with clear relationships between wake dynamics (typically characterised by particle Reynolds or Galileo number) and density ratio [11,13], geometry [14] or dimensionless inertia [16,30,31]. However, no equivalent framework currently exists for river litter, nor is there a mechanistic explanation of its dynamics, despite the wide range of dimensionless parameters (spanning up to four orders of magnitude beyond previous investigations for canonical particles [11,16,17]), resulting from the vast diversity of litter physical properties.

To solve this knowledge gap, we provide a complete, mechanistic description of the settling and rising dynamics of full-scale riverine litter under quiescent conditions. Combining two large-scale settling facilities (Fig. 1a) and employing a synchronised multi-camera setup, we reconstruct the three-dimensional trajectories of 1,011 fully representative pristine, deformed, and weathered litter items, representing 80% of the most commonly observed River-OSPAR (Oslo and Paris commission) categories (Fig. 1b) [26]. We (*i*) quantify the empirical bounds of litter settling and rising velocities, together with their drag coefficients; (*ii*) characterize four distinct trajectory regimes

(straight vertical, straight oblique, nonlinear vertical, and nonlinear oblique) (Fig. 1c-f); (*iii*) establish a predictive regime map based on particle Reynolds number and litter anisotropy and (*iv*) provide the missing mechanistic interpretation of litter vertical transport in quiescent water, thereby resolving the hydrodynamic parameters required for physics-based transport models.

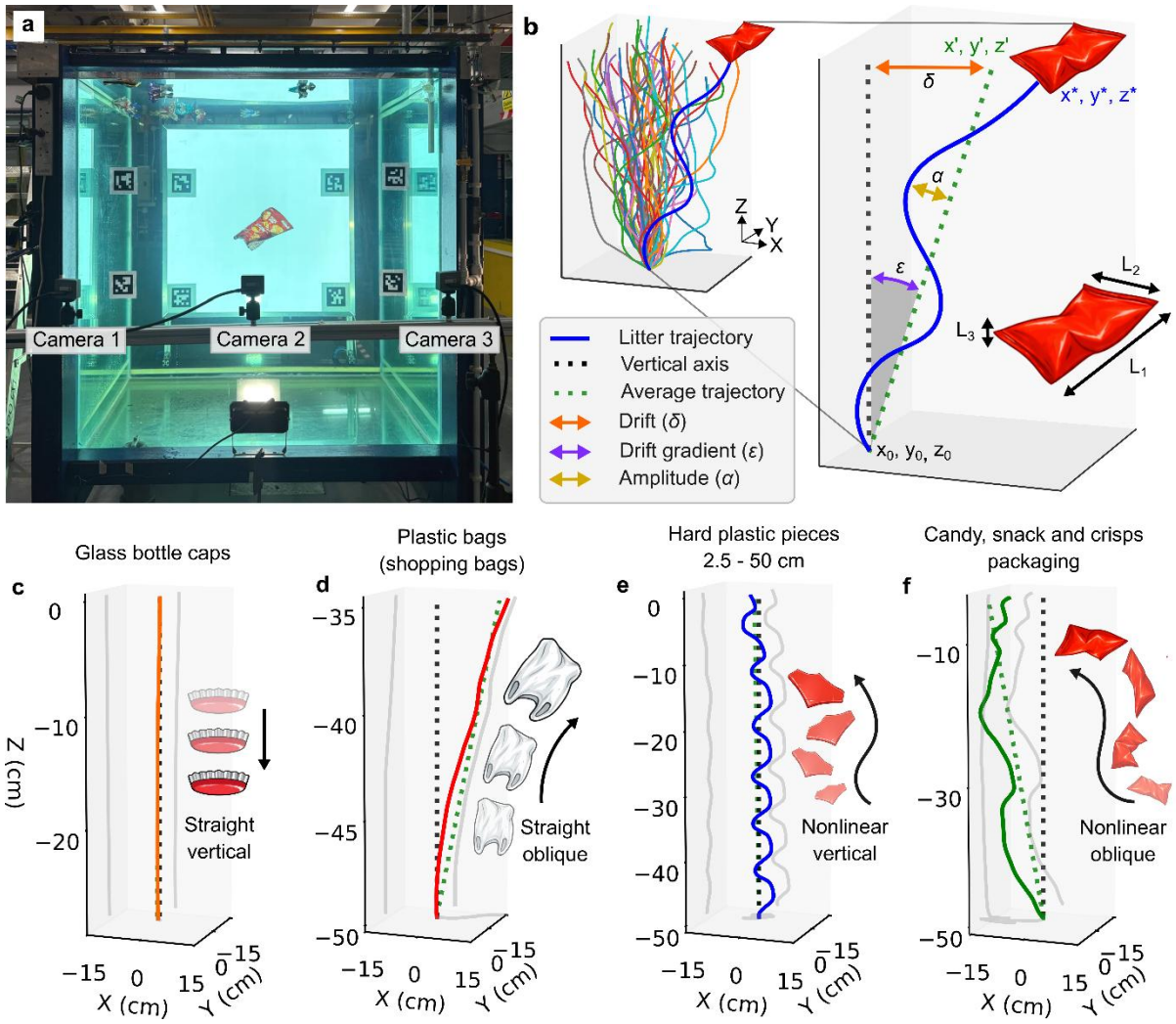

Fig. 1 | Experimental framework and trajectory regimes of settling and rising litter. a) Settling tank (Tank 2) and camera configuration enabling three-dimensional trajectory reconstruction with millimetre accuracy. **b)** Parametrisation of trajectory dynamics including drift (δ), drift gradient (ε) and amplitude (α). **c-f)** Settling and rising trajectory regimes: **c)** straight vertical, **d)** straight oblique, **e)** nonlinear vertical, **f)** nonlinear oblique.

2 Methods

2.1 Litter items

Litter items tested for experiments comprise 24 of the 25 most persistent River-OSPAR categories found in rivers and on riverbanks, representing approximately 80% of all riverine litter. This selection is drawn from the dataset compiled by [26], which synthesises river and riverbank litter

observations from 22 study sites across four continents, such as [32–35]. Only one category ('Other litter') from the top 25 most frequently observed River-OSPAR categories was omitted from experiments because the variability in size, density, and mass within this category was too large to allow meaningful testing.

Items consisted of pristine, deformed, and weathered litter and captured the variability typical of river litter (see Supplementary Fig. 1 for validation). Pristine items were newly purchased and tested without damage, whereas deformed items were altered from their original state (e.g., cut fragments or crushed plastic bottles) to replicate common environmental degradation. Weathered items were collected directly from the urban environment and tested in their existing condition. Between 29 and 67 individual litter items per River-OSPAR category were tested, resulting in a total of 1,011 trajectories across all categories. The tested River-OSPAR categories and the ranges of their geometric and material properties are provided in Supplementary Table 1.

2.2 Litter physical properties

For each item, mass (M), volume (V), and density (ρ_p) were determined. The mass of each item was measured to an accuracy of 0.001 g for lighter litter, and 0.1 g for heavier litter. The dry mass was used for non-absorbent litter items and wet mass for absorbent items (i.e. wet wipes and cotton swabs), once at equilibrium absorbance. Material and effective density and volume were determined experimentally where possible using buoyant weighing (Archimedes principles) or a gas pycnometer. A full description of density and volume measurements is provided in the Supplementary Methods.

The longest (L_1), intermediate (L_2) and shortest dimensions (L_3) of the items were measured with a tape measure. When an item's shortest dimension was too small to be measured with a tape measure (< 1 mm), such as for plastic films or wet wipes, L_3 was estimated through the item's volume (i.e. $L_3 = V / (L_1 L_2)$). Measuring the items principal dimensions allow for their flatness ($FL = L_3/L_2$), elongation ratio ($EL = L_2/L_1$) and Corey shape factor [36] ($CSF = L_3/\sqrt{L_1 L_2}$) to be calculated, which define the litter's geometric anisotropy.

2.3 Settling tanks and camera setup

Experiments were conducted in two settling tanks. Small litter which demonstrated straight vertical trajectories and had little interactions with the tank walls were tested in a rectangular settling tank (Tank 1), 98 cm in height, 200 cm in length and 57 cm in width at the Theodor Rehbock Hydraulics Laboratory at Karlsruhe Institute of Technology (Germany). Larger litter, which exhibited significant horizontal drift and amplitudes, and could have led to wall

interactions in Tank 1, were measured in a 128 cm cuboidal settling tank (Tank 2, Fig. 1A) at the Hydrodynamics Laboratory at Imperial College London (United Kingdom). Three Baumer VLXT-81C.I cameras (2/3" CMOS sensor, 2848 × 2832 px^2, 60 FPS) were positioned to record litter trajectories in Tank 1, while three OBSBOT Meet 2 cameras (1/2" CMOS sensor, 1980 × 1080 $pixel^2$, 60 FPS) were used in Tank 2. Full description of camera specifications and set up is provided in the Supplementary Methods.

2.4 Release protocol

Litter items were released individually into the settling tanks. Negatively buoyant items were released just below the water surface by hand, whereas positively buoyant items were released from the bottom of the tank using a 2.4 m-long grabber. When the grabber orientation allowed, items were released at random orientations to capture the full range of settling or rising dynamics of the litter items. Care was taken during each release to minimise external disturbances in the tank that could introduce bias in the initial orientation or motion of the item.

Prior to release, items were gently agitated to remove air bubbles adhering to their surfaces or internal voids and the experiment did not start until free surface disturbances vanished. To improve contrast with the background during image detection, transparent and translucid items were marked using blue or black marker pen, resulting in less than 1% change in item mass [37]. Once released, litter items travelled at least 15 cm through the water column, reaching a stable orientation and motion independent of release conditions before tracking was initiated.

2.5 Litter tracking and three-dimensional reconstruction

A bounding box detection routine, using the Python library OpenCV [38], was used to capture the litter's contour and centre-of-mass position per frame from each of the three camera's video sequence, similar to [8,39,40]. The 2D image coordinates of the litter obtained from three cameras were used to reconstruct the litter's 3D centre-of-mass position (x, y, z) in the tank via ray-intersection triangulation, accounting for refraction across the air–glass–water interfaces, following methods by [41] and described in full in [8]. Camera extrinsic parameters were calibrated using ArUco markers mounted on the front wall of the tank. Reconstruction accuracy was evaluated by comparing the known spatial coordinates of ArUco markers mounted on the front and back walls with their reconstructed positions. Across all experiments, mean absolute reconstruction errors were below 8 mm, with a standard deviation less than 3 mm in each coordinate direction. This procedure yielded vertical litter trajectories of approximately 35 cm in Tank 1 and 50 cm in the larger Tank 2. A detailed description of the 3D reconstruction algorithm

and trajectory smoothing is provided in the Supplementary Methods while an exemplary detection and reconstruction routine is provided in [42]

2.6 Trajectory characterisation

The vertical velocity (w) for each trajectory was calculated for each trajectory as the net vertical displacement divided by the corresponding time interval over the entire trajectory.

$$w = \frac{z_* - z_0}{t_* - t_0} \quad \text{(Eq. 1)}$$

where z_0 and z_* are the initial and final vertical positions of the trajectory (Fig. 1 b), and t_0 and t_* are the corresponding times.

To quantify lateral drifting motions, two linear regressions were fitted to the litter trajectory in the $x - z$ and $y - z$ planes using ordinary least squares, treating z as the independent variable. The resulting fits define a linear mean trajectory in three-dimensional space. This provides a consistent reference for quantifying the litter's trajectory dynamics (Fig. 1b). The lateral drift (δ) of each litter item can then be defined as the Euclidean distance between the particle's initial coordinates (x_0, y_0) and the average trajectory's final coordinates (x', y') in the horizontal plane:

$$\delta = \sqrt{(x' - x_0)^2 + (y' - y_0)^2} \quad \text{(Eq. 2)}$$

which yields the drift velocity (v):

$$v = \frac{\delta}{t_* - t_0} \quad \text{(Eq. 3)}$$

To quantify the litter's nonlinear motion, the amplitude of the trajectory (α) was defined as the standard deviation of lateral displacements between the measured trajectory and the linear regression-based average trajectory (Fig. 1b). This is calculated by projecting the horizontal displacement vector at each vertical position onto the direction perpendicular to the overall drift. Thus, α is a measure of how strongly the trajectory departs from a straight linear path, with larger values indicating greater deviation.

3 Results

3.1 Vertical and lateral velocities of river litter

Across all River-OSPAR litter items, vertical velocities in quiescent conditions ranged between -82.1 and -0.29 cm s^{-1} for rising litter and 0.90 and 143.3 cm s^{-1} for settling litter (Fig. 2a). Vertical velocities were largely explained by their material density ρ_p. Litter composed of near-neutrally buoyant materials (ρ_p = 0.8 - 1.5 g cm^{-3}), which represent the most frequently observed River-

OSPAR litter categories in rivers [26] – plastics (PO soft, PO hard, PET, PS), multilayer, paper and textiles – exhibited rising velocities between -0.29 and -21.1 cm s^{-1} and settling velocities between 0.90 and 16.3 cm s^{-1}. Dense glass and metal (ρ_p > 2.5 g cm^{-3}) litter, such as metal beverage cans and glass bottles, held the fastest vertical settling velocities between 8.8 and 143.3 cm s^{-1}, while buoyant expanded polystyrene (EPS) (ρ_p < 0.08 g cm^{-3}) litter displayed the fastest rising velocities between -7.4 and -82.1 cm s^{-1}.

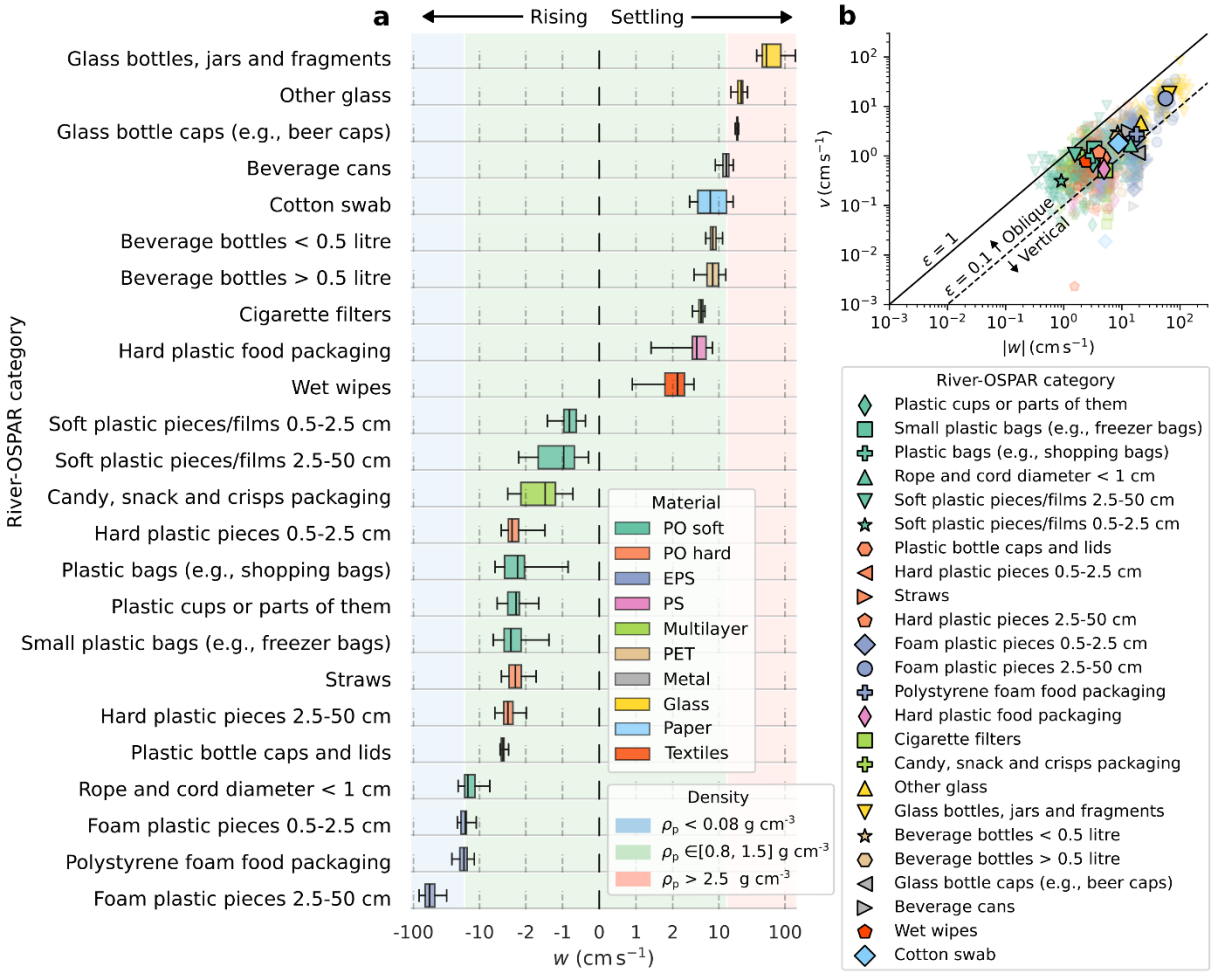

Fig. 2 | Vertical rising and settling velocities of the most persistent River-OSPAR litter categories in river environments. a) Log-scale boxplots of the vertical velocities (w). Box colours denote the material composition of the litter items. Background shading indicates approximate velocity ranges associated with a material density (ρ_p) range, approximated using the median settling or rising velocities (central lines of the boxplots) of categories located at the boundaries between density classes. **b**) Absolute vertical velocities ($|w|$) plotted against lateral velocities (v), dashed lines indicate the drift gradient $\varepsilon = v/|w|$ delineating vertical (ε > 0.1) and oblique (ε < 0.1) trajectories.

Fig. 3 shows the drag coefficients (C_D) of the tested litter items. Despite the wide variability of litter velocities (Fig. 2a) and litter physical properties, C_D values remain relatively consistent

within a relatively narrow range across River-OSPAR categories. Across all tested items, the median drag coefficient was 1.03, with an interquartile range spanning 0.45 to 1.72. A detailed statistical breakdown of C_D by River-OSPAR category is provided in Supplementary Table 2.

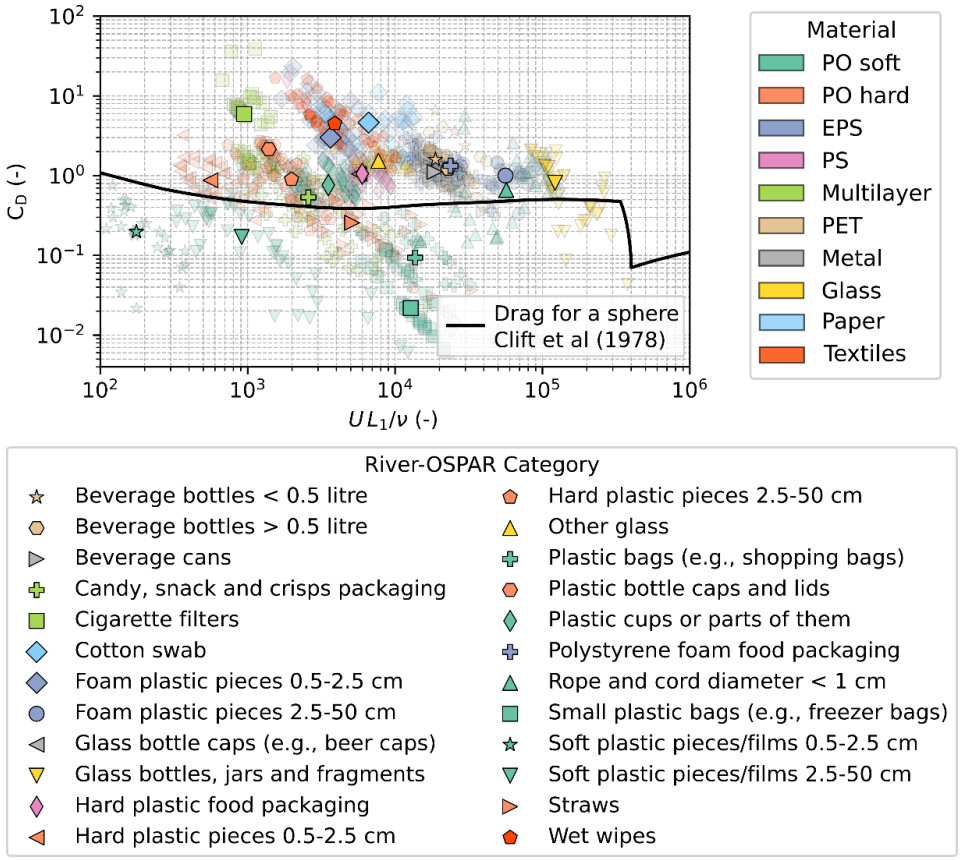

Fig 3. | Drag coefficients (C_D) for river litter. Calculated drag coefficient (C_D) plotted against a Reynolds number calculated with the velocity magnitude $U = \sqrt{w^2 + v^2}$ and the longest length of the litter item (L_1). Faint markers denote individual litter values, coloured by their material composition. Bold markers represent River-OSPAR category median. Black line represents a drag coefficient for a sphere[43]

Drift velocities (v) for litter ranged between 0.002 and 83 cm s^{-1} and tended to increase with the absolute value of the vertical velocity ($|w|$) (Fig.2b), indicating that part of the buoyancy force induces lateral dispersion. To quantify the relative importance of vertical versus lateral velocities, we calculate the drift gradient ($\varepsilon = v/|w|$), which is the rate of horizontal displacement per unit vertical movement, where smaller ε values indicate trajectories dominated by vertical motion with limited horizontal displacement, whereas values approaching 1 indicate vertical and drift velocities of similar magnitudes (i.e. a trajectory at a 45° slope).

Average drift gradients ε across River-OSPAR categories were all below 1, confirming that litter movement was mainly vertically dominated. Considering a threshold of ε > 0.1 to distinguish

straight vertical trajectories from drifting trajectories, we observe the that 78% of all litter items exhibited $\varepsilon > 0.1$. These results demonstrates that lateral motion is a substantial component of litter's transport, typically exceeding the drift gradients documented for canonical spheres [11], cylinders [14] and steady or oscillating disks [31,44].

3.2 Dynamics of river litter

Each of the 1,011 reconstructed trajectories was classified into four regimes based on the drift gradient (ε) and deviations from a straight-line trajectory, quantified by the normalised amplitude (α/L_1) (see Methods): straight vertical ($\varepsilon < 0.1$, $\alpha/L_1 < 0.05$; Fig. 1c), straight oblique ($\varepsilon > 0.1$, $\alpha/L_1 < 0.05$; Fig. 1d), nonlinear vertical ($\varepsilon < 0.1$, $\alpha/L_1 \geq 0.05$; Fig. 1e), and nonlinear oblique ($\varepsilon > 0.1$, $\alpha/L_1 \geq 0.05$; Fig. 1f). We then examined the predominant trajectory regime within each River-OSPAR category, defined as the regime accounting for ≥ 50% of trajectories for that category (Supplementary Fig. 2). Across the 24 River-OSPAR categories tested, straight oblique trajectories constituted the dominant regime in nine categories (38%). Nonlinear oblique trajectories were the second most dominant regime, occurring in eight categories (33%). In contrast, only two (8%) categories showed a dominant straight vertical regime, whereas one (4%) category exhibited a dominant nonlinear vertical regime. Four categories (17%) were classified as mixed, where no dominant mode was observed.

We observed that normalised litter drift (δ) and amplitude (α), tended to decrease with increasing Reynolds number ($\mathrm{Re_p} = w\,L_1/\nu$) (Fig. 4). The same trend is observed when data is plotted against the particle Galileo number (Supplementary Fig. 3), which is commonly used to characterise dynamics of spheres [11–13] and disks [15,45]. This indicates that the trajectory dynamics are primarily governed by particle inertia relative to viscous effects, independently of whether the forcing mechanism is velocity-driven or buoyancy-driven.

Nonlinear trajectories predominantly occur across intermediate Reynolds numbers ($\mathrm{Re_p} \approx 100$ to 3,000), consistent with the emergence of unsteady laminar-to-transitional wake dynamics. In this regime, coherent vortices that generate lateral forces on the litter body are shed at scales comparable to the litter scale [11,27,31]. This drives drift and oscillation amplitudes of litter in the order of $\delta/L_1 \approx 0.3$ to 3 (Fig. 4a) and $\alpha/L_1 \approx 0.05$ to 1 (Fig. 4b). Above $\mathrm{Re_p} \approx 3{,}000$, trajectories become straighter, with δ/L_1 typically falling < 0.3 and α/L_1 frequently < 0.05. This behaviour is consistent with wake-transition behaviour reported for freely moving bodies [27] where, for increasing turbulence levels, the progressive loss of coherency of the wake-generated vortices reduces effective lateral forces on the object.

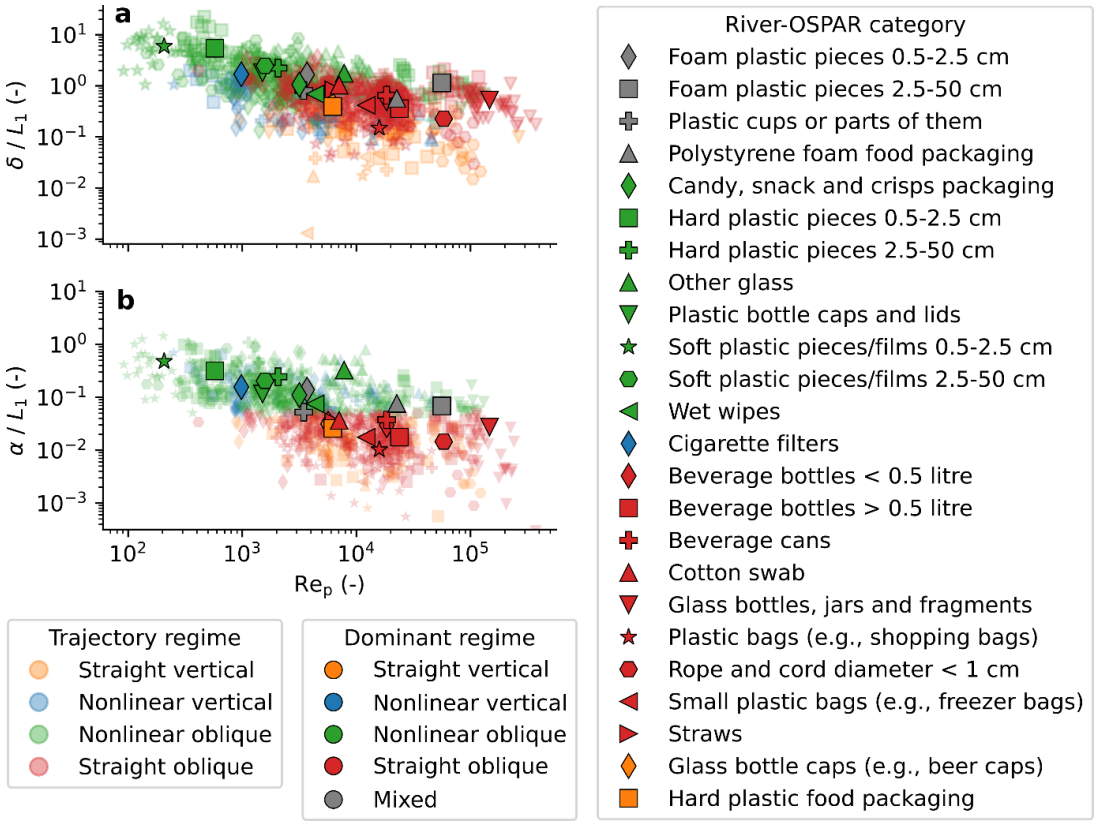

Fig. 4 | Drifting and nonlinear dynamics of river litter. Scatter plots of litter **a)** drift (δ) and **b)** amplitude (α), normalised by the longest dimension of the litter (L_1), as a function of the particle Reynolds number ($\mathrm{Re_p}$). Faint markers denote individual litter trajectories, coloured by their classified trajectory regime (straight vertical, straight oblique, nonlinear vertical and nonlinear oblique). Bold markers represent River-OSPAR category mean, coloured by their dominant regime.

These observations extend previously described trajectory regimes to Galileo and Reynolds numbers more than four orders of magnitude higher than earlier work on canonical objects. Unlike studies of spheres or disks, where motion becomes increasingly nonlinear or chaotic as Ga or Re increases, our results indicate that litter may reach an asymptotic behaviour at very high inertia. For example, steady, straight motion has only been described for spheres at $\mathrm{Ga} < 200$ [11–13] and for disks at $\mathrm{Re_p} < 100$ [16,30,31] in prior studies. In contrast, we find that such steady regimes reappear at values nearly two orders of magnitude higher.

3.3 Regime map for river litter

To connect fluid-mechanics descriptors with litter geometry, we first plot the drift gradient (ε) against the particle Reynolds number ($\mathrm{Re_p}$), where the four identified trajectory regimes become evident (Fig. 5a). These regimes are then projected onto geometrical descriptors defined by

flatness ($FL = L_3/L_2$) and elongation ratios ($EL = L_2/L_1$) (Fig. 5b-f), allowing trajectory regimes to be interpreted through measurable shape parameters.

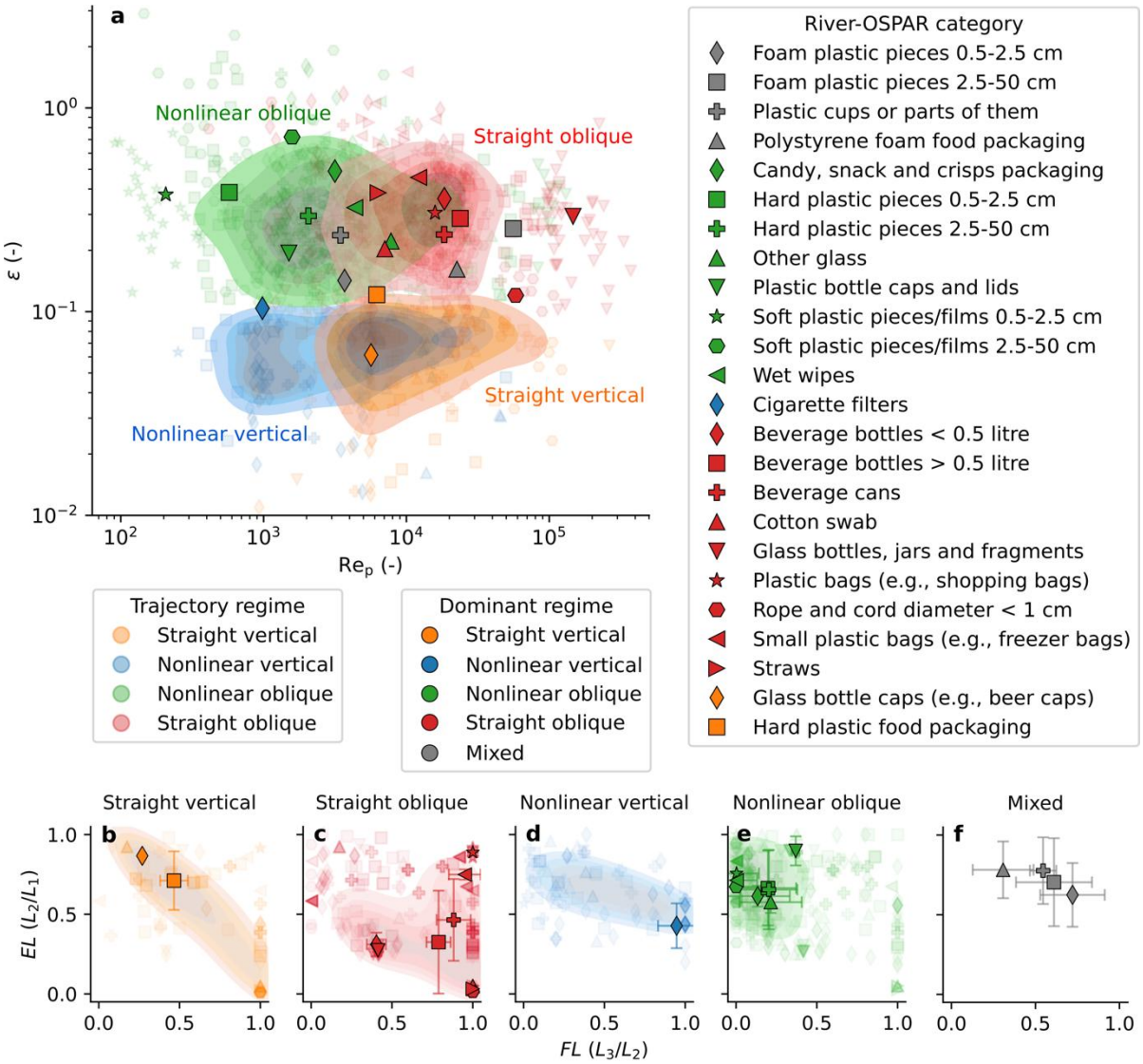

Fig. 5 | Regime map of settling or rising river litter. a) Drift gradient $\varepsilon = v/|w|$ plotted against the particle Reynolds number ($\mathrm{Re_p}$) for all trajectories. Bivariate KDE map (bandwidth = 1) delineates the four trajectory regimes: straight vertical, straight oblique, nonlinear vertical and nonlinear oblique. Faint markers denote individual litter trajectories, coloured by their classified trajectory regime. Bold makers represent category means for each River-OSPAR category. **b – f)** Dominant trajectory regimes in the litter geometry space, defined by flatness ($FL = L_3/L_2$) and elongation ratios ($EL = L_2/L_1$).

Two distinct mechanisms govern the identified trajectory regimes: the wake dynamics, which drives the emergence of nonlinear motion, and geometric anisotropy, associated with uneven principal moments of inertia, which governs the oblique motion of litter. At $\mathrm{Re_p}$ < 3,000 and ε > 0.1, nonlinear oblique trajectories dominate. Items in this regime are primarily small, with low

effective mass (e.g., small plastic films and fragments). Due to their small effective mass, these items are highly responsive to laminar-to-transitional wake-induced vortex shedding, producing amplitudes of the order of magnitude of their size (Fig. 4b) and motion more frequently classified as nonlinear.

All items in the nonlinear oblique region present flat, anisotropic geometries (FL < 0.4, EL = 0.5–0.8) (Fig. 5e). For such items, inclination relative to the main direction of motion generates asymmetric pressure distributions that yield lift forces, inducing lateral motion [46]. The combination of wake sensitivity and geometry-driven rotational asymmetry promotes nonlinear oblique trajectories. Uneven mass distributions may produce similar effects or further amplify them, as demonstrated by biofouled plastic items [39].

At $\mathrm{Re_p}$ > 3,000 and ε > 0.1, trajectories transition toward straight oblique motion (Fig. 5a). Litter in this regime are associated with larger litter items with more effective mass (e.g., water-filled plastic bags, plastic bottles, and glass bottles). Their greater effective mass reduces sensitivity to increasingly incoherent wake structures. As a result, these litter items display small amplitudes relative to their size, displaying trajectories which are more frequently classified as straight. Despite straight trajectories, these items remain anisotropic in shape (e.g., plastic bottles, cotton swabs and straws), generating lift forces that drive oblique motion (Fig. 5c). Plastic bags are a notable exception because they deform during motion and adopt geometries that differ from their measured dimension. Consequently, drift persists, but trajectories remain straight.

A notable deviation is observed for low-density expanded polystyrene (EPS) items, such as foam food packaging and foam fragments. At $\mathrm{Re_p}$ values comparable to larger litter with straight oblique paths (e.g., plastic bags or bottles), EPS items more frequently exhibit nonlinear or mixed trajectories (Fig. 5a). Although their particle Reynolds numbers are similar, their masses are up to three orders of magnitude smaller. Consequently, EPS items of a given size experience similar hydrodynamic forcing but respond more rapidly to wake instabilities due to their lower inertia. Their large buoyancy also promotes higher vertical velocities, which further enhances wake instabilities, producing sustained nonlinear movements. This leads to more diverse and variable trajectories, and their overall dominant regime is classified as mixed.

For ε < 0.1, vertical motion dominates and litter trajectories become predominantly straight, independently of $\mathrm{Re_p}$. Litter in this region are generally more isotropic (Fig. 5 b, d), which may be linked to a more symmetric pressure and drag distribution about their centre of mass. This isotropy likely corresponds to more evenly distributed principal moments of inertia, such that hydrodynamic forcing remains balanced and no persistent lateral motion develops. Within this non-oblique regime, two regimes emerge, separated at $\mathrm{Re_p} \approx 3{,}000$. At lower $\mathrm{Re_p}$, litter remains sensitive to laminar-to-transitional wake forcing and therefore exhibits more nonlinear trajectories (e.g. cigarette filters). At higher $\mathrm{Re_p}$, wake production becomes less effective at displacing denser items (e.g., metal bottle caps) or larger rigid litter (e.g., polystyrene packaging), and motion becomes predominantly straight. The transition between straight and nonlinear behaviour in this region thus reflects differences in wake responsiveness rather than geometric anisotropy.

4 Discussion

The resulting dataset produced from these experiments [42] can be used in practice as inputs for population balance models [47] or to directly explain the vertical distribution of litter in hydrodynamically characterised rivers [7–9], through calculation of the Rouse number [48]. For instance, it would be expected that near-neutrally buoyant litter items, such as small plastic films and fragments with low vertical velocities and large drift gradients (Fig. 2), to remain suspended and highly dispersed within the water column, where their distribution is governed primarily by turbulent mixing rather than buoyancy-driven transport. Conversely, dense glass and metal litter with high settling velocities will remain concentrated near the bed or largely immobile with limited downstream dispersion. On the other hand, highly buoyant EPS will persist on the surface and be rapidly transported downstream. Interpreting our results in this way directly improves predictions of litter transport pathways for varying properties of riverine litter, providing physics-based approaches to identify litter hotspots, design representative monitoring strategies, and deploy effective in-stream interception infrastructure. This work resolves the missing particle-scale dynamics and mechanistic explanation required for a physical understanding of litter transport through the environment, enabling the development of solutions aimed at reducing their ecological and human impacts.

Data availability statement

Full litter data set, including litter properties, dimensionless numbers and velocities.

Summary dataset with key statistics

Code availability

Litter detection and reconstruction codes available at https://doi.org/10.5281/zenodo.19203455

Acknowledgements

Alexander von Humboldt Foundation Research Fellowship

Contributions

James Lofty: Conceptualization, Investigation, Writing – Original Draft.

Daniel Valero: Conceptualization, Supervision. Writing - Review & Editing

Mario Franca: Conceptualization, Supervision. Writing - Review & Editing

Competing interests

The authors declare no competing interests.

References

1. Clark, B. L. *et al.* Global assessment of marine plastic exposure risk for oceanic birds. *Nat. Commun.* **14**, 3665 (2023).
2. MacLeod, M., Arp, H. P. H., Tekman, M. B. & Jahnke, A. The global threat from plastic pollution. *Science (1979).* **373**, 61–65 (2021).
3. Honingh, D. *et al.* Urban River Water Level Increase Through Plastic Waste Accumulation at a Rack Structure. *Front. Earth Sci. (Lausanne).* **8**, (2020).
4. Beaumont, N. J. *et al.* Global ecological, social and economic impacts of marine plastic. *Mar. Pollut. Bull.* **142**, 189–195 (2019).
5. Meijer, L. J. J., Emmerik, T. van, Ent, R. van der, Schmidt, C. & Lebreton, L. More than 1000 rivers account for 80% of global riverine plastic emissions into the ocean. *Sci. Adv.* **7**, eaaz5803 (2021).
6. van Emmerik, T., Mellink, Y., Hauk, R., Waldschläger, K. & Schreyers, L. Rivers as Plastic Reservoirs. *Frontiers in Water* **3**, 786936 (2022).
7. Lofty, J. *et al.* On the vertical structure of non-buoyant plastics in turbulent transport. *Water Res.* **254**, 121306 (2024).
8. Valero, D., Belay, B. S., Moreno-Rodenas, A., Kramer, M. & Franca, M. J. The key role of surface tension in the transport and quantification of plastic pollution in rivers. *Water Res.* **226**, 119078 (2022).
9. Cowger, W., Gray, A. B., Guilinger, J. J., Fong, B. & Waldschläger, K. Concentration Depth Profiles of Microplastic Particles in River Flow and Implications for Surface Sampling. *Environ. Sci. Technol.* **55**, 6032–6041 (2021).
10. González-Fernández, D., Roebroek, C. T. J., Laufkötter, C., Cózar, A. & van Emmerik, T. H. M. Diverging estimates of river plastic input to the ocean. *Nature Reviews Earth & Environment 2023 4:7* **4**, 424–426 (2023).
11. Jenny, M., Dušek, J. & Bouchet, G. Instabilities and transition of a sphere falling or ascending freely in a Newtonian fluid. *J. Fluid Mech.* **508**, 201–239 (2004).

12. Raaghav, S. K. R., Poelma, C. & Breugem, W. P. Path instabilities of a freely rising or falling sphere. *International Journal of Multiphase Flow* **153**, 104111 (2022).
13. Cabrera-Booman, F., Plihon, N. & Bourgoin, M. Path instabilities and drag in the settling of single spheres. *International Journal of Multiphase Flow* **171**, 104664 (2024).
14. Toupoint, C., Ern, P. & Roig, V. Kinematics and wake of freely falling cylinders at moderate Reynolds numbers. *J. Fluid Mech.* **866**, 82–111 (2019).
15. Auguste, F., Magnaudet, J. & Fabre, D. Falling styles of disks. *J. Fluid Mech.* **719**, 388–405 (2013).
16. Field, S. B., Klaus, M., Moore, M. G. & Nori, F. Chaotic dynamics of falling disks. *Nature* **388**, 252–254 (1997).
17. Smith, E. H. Autorotating wings: an experimental investigation. *J. Fluid Mech.* **50**, 513–534 (1971).
18. Anderson, A., Pesavento, U. & Wang, Z. J. Unsteady aerodynamics of fluttering and tumbling plates. *J. Fluid Mech.* **541**, 65 (2005).
19. Waldschläger, K. & Schüttrumpf, H. Effects of Particle Properties on the Settling and Rise Velocities of Microplastics in Freshwater under Laboratory Conditions. *Environ. Sci. Technol.* **53**, 1958–1966 (2019).
20. Goral, K. D. *et al.* Settling velocity of microplastic particles having regular and irregular shapes. *Environ. Res.* **228**, 115783 (2023).
21. Yu, Z., Yang, G. & Zhang, W. A new model for the terminal settling velocity of microplastics. *Mar. Pollut. Bull.* **176**, 113449 (2022).
22. Khatmullina, L. & Isachenko, I. Settling velocity of microplastic particles of regular shapes. *Mar. Pollut. Bull.* **114**, 871–880 (2017).
23. Kuizenga, B., Van Emmerik, T., Waldschläger, K. & Kooi, M. Will it Float? Rising and Settling Velocities of Common Macroplastic Foils. *ACS ES and T Water* **2**, 975–981 (2022).
24. Born, M. P., Junge, L. V., Brüll, C., Waldschläger, K. & Schüttrumpf, H. Terminal settling and rising velocity prediction of macroplastics: Medical face masks as newly emerged objects of concern. *Science of The Total Environment* **908**, 167922 (2024).
25. Royer, S. J. *et al.* Rise velocity of small polyolefin plastics in a seawater tank exposed to natural conditions in Hawai'i. *Environ. Res. Commun.* **7**, 095018 (2025).
26. Lofty, J., Rebai, D., Valero, D. & Franca, M. J. The Shapes and Sizes of Macroplastics and Other Litter in Rivers. *Environ. Sci. Technol.* https://doi.org/10.1021/acs.est.5c13126 (2026) doi:10.1021/acs.est.5c13126.
27. Ern, P., Risso, F., Fabre, D. & Magnaudet, J. Wake-Induced Oscillatory Paths of Bodies Freely Rising or Falling in Fluids. *Annu. Rev. Fluid Mech.* **44**, 97–121 (2012).
28. Voth, G. A. & Soldati, A. Anisotropic Particles in Turbulence. *https://doi.org/10.1146/annurev-fluid-010816-060135* **49**, 249–276 (2017).
29. Baker, L. J. & Coletti, F. Experimental investigation of inertial fibres and disks in a turbulent boundary layer. *J. Fluid Mech.* **943**, A27 (2022).
30. Willmarth, W. W., Hawk, N. E. & Harvey, R. L. Steady and Unsteady Motions and Wakes of Freely Falling Disks. *Phys. Fluids* **7**, 197–208 (1964).
31. Stringham, G. E., Simons, D. B., Guy, H. P. & Pecora, W. T. The Behavior of Large Particles Falling in Quiescent Liquids. *US Government Printing Office* (1969).
32. van Emmerik, T. *et al.* Riverbank macrolitter in the Dutch Rhine–Meuse delta. *Environmental Research Letters* **15**, 104087 (2020).
33. Tramoy, R., Colasse, L., Gasperi, J. & Tassin, B. Plastic debris dataset on the Seine river banks: Plastic pellets, unidentified plastic fragments and plastic sticks are the Top 3 items in a historical accumulation of plastics. *Data Brief* **23**, 103697 (2019).
34. Ballerini, T. *et al.* Plastic pollution on Durance riverbank: First quantification and possible environmental measures to reduce it. *Frontiers in Sustainability* **3**, 866982 (2022).

35. de Lange, S. I. *et al*. Sample size requirements for riverbank macrolitter characterization. *Frontiers in Water* **4**, (2023).
36. Corey, A. T. *et al*. Influence of shape on the fall velocity of sand grains. https://doi.org/10.17616/R31NJMSY (1949) doi:10.17616/R31NJMSY.
37. Valero, D., Felder, S., Seidel, F., Moreno-Rodenas, A. & Franca, M. J. Low-intrusive colour-enhanced pattern coating of plastics for fluid-mechanics laboratory experiments. *EGU General Assembly* 8159 Preprint at https://doi.org/10.5194/egusphere-egu24-8159 (2025).
38. Bradski, G. The openCV library. *Dr. Dobb's Journal: Software Tools for the Professional Programmer* **25**, 120–123 (2000).
39. Lofty, J., Wilson, C. & Ouro, P. Biofouling changes the settling dynamics of macroplastic plates. *Commun. Earth Environ.* **5**, 750 (2024).
40. Lofty, J. *et al*. Three-Dimensional Settling Dynamics of Environmental Microplastics. *Environ. Sci. Technol.* https://doi.org/10.1021/ACS.EST.5C12960 (2026) doi:10.1021/ACS.EST.5C12960.
41. Duinmeijer, S. P. A. *et al*. A simple measuring set-up for the experimental determination of the dynamics of a large particle in the 3D velocity field around a free surface vortex. *Flow Measurement and Instrumentation* **65**, 52–64 (2019).
42. Lofty, J. JamesLofty/Settling_rising_litter_dataset: Settling_rising_litter_dataset_v1. https://doi.org/10.5281/ZENODO.19203455 (2026) doi:10.5281/ZENODO.19203455.
43. Clift, R., Grace, J. R. & Weber, M. E. Bubbles, Drops, and Particles (Dover Civil and Mechanical Engineering). 380 (1978).
44. Fernandes, P. C., Risso, F. D., Ern, P. & Magnaudet, J. Oscillatory motion and wake instability of freely rising axisymmetric bodies. *J. Fluid Mech.* **573**, 479–502 (2007).
45. Tinklenberg, A., Guala, M. & Coletti, F. Thin disks falling in air. *J. Fluid Mech* **962**, (2023).
46. Mandø, M. & Rosendahl, L. On the motion of non-spherical particles at high Reynolds number. *Powder Technol.* **202**, 1–13 (2010).
47. Shettigar, N. A., Bi, Q. & Toorman, E. Assimilating Size Diversity: Population Balance Equations Applied to the Modeling of Microplastic Transport. *Environ. Sci. Technol.* **58**, 16112–16120 (2024).
48. Rouse, H. An Analysis of Sediment Transportation in the Light of Fluid Turbulence. https://resolver.caltech.edu/CaltechAUTHORS:20140529-132455484 (1939).